Experimental and Numerical Analysis of Incompressible Flow over an Iced Airfoil

Karima E. Amori **Ethar Saad Ahmed**
Professor
College of Engineering-University of Baghdad
drkarimaa@yahoo.com ethar_eng_87@yahoo.com

ABSTRACT

Determining the aerodynamic characteristics of iced airfoil is an important step in aircraft design. The goal of this work is to study experimentally and numerically an iced airfoil to assess the aerodynamic penalties associated with presence of ice on the airfoil surface. Three iced shapes were tested on NACA 0012 straight wing at zero and non-zero angles of attack, at Reynolds No. equal to ($3.36*10^5$). The 2-D steady state continuity and momentum equations have been solved utilizing finite volume method to analyze the turbulent flow over a clean and iced airfoil. The results show that the ice shapes affected the aerodynamic characteristics due to the change in airfoil shape. The experimental results show that the horn iced airfoil consumes more power than the other shapes of ice, its value was (44.4W). The horn iced shape has the worst effect on the airfoil than the other shapes. The present results are compared with previously reported results; it is found there is a very good agreement between them. A comparison between the experimental and computational results of the presented work were pursing the same behavior.

Keywords : Iced airfoil, computational fluid dynamics, turbulence model, drag, lift, aerodynamic.

التحليل التجريبي والعددي لجريان لاانضغاطي حول مطيار مثلج

أ.د. كريمة أسماعيل عموري **ايثار سعد أحمد**

الخلاصة

إن تحديد الخصائص الديناميكية الهوائيه لمطيار متكون عليه جليد هو خطوة هامة في تصميم الطائرات. الهدف من هذا العمل هو بناء تجارب عملية وعددية لجنيح متجمد وذلك لتقييم الاداء الايروديناميكي المرتبط بوجود ثلج على سطح الجنيح.تم اختيار ثلاثة اشكال لثلج متكون على مطيار من نوعNACA 0012 حيث اختبرت عند زاويا هجوم صفرية غير صفرية ولعدد رينولدز($3.36*10^5$). تم حل معادلات الاستمرارية والزخم ذات البعدين للحاله المستقرة باستخدام طريقة الحجوم المحددة وذلك لتحليل الجريان المضطرب حول جنيح بدون ومع وجود الثلج عليه.أظهرت النتائج إن اشكال الثلج المتولده على المطيار تؤثر على الخصائص الايروديناميكية وذلك بسبب تغير الشكل الانسيابي للجنيح. النتائج التجريبية بينت أن شكل الثلج بحافة حادة على الجنيح يستهلك طاقة اعلى من بقية اشكال الثلج, حيث كانت أعظم طاقة (44.4 واط). أظهرت النتائج ايضا أن الثلج ذو الحافة الحادة تأثيره الاسوء على الأجنحة من بقية الاشكال.قورنت النتائج الحالية مع نتائج لبحوث سابقة وكانت متوافقة معها بصورة جيدة جدا. قورنت النتائج العملية مع النتائج النظرية، حيث كانت تسلك نفس السلوك .

1. INTRODUCTION

Decades of operational experiences have revealed many situations in flight as well as on the ground when ice can accrete on ‘‘ice-protected’’ aircraft. With the very large variety of forms and sizes in which ice can accrete on aircraft surfaces in real operational conditions, the challenge facing researchers and aircraft designers has been to establish an effective process for defining the accretion process and physical characteristics of these ice shapes for any aircraft surface at any flight or meteorological conditions, and to determine which are the most harmful iced shape. Typically, some flight testing in natural icing conditions is required as part of the aircraft certification process for new aircraft designs in order to demonstrate the effectiveness of ice protection systems as well as overall aircraft performance and handling characteristics. In the late 80’s of the previous century, several studies have been completed of ice accretions and resulting performance losses for airfoil profiles by National Air and Space Administration (NASA) Lewis research which led to many important works. Many researchers investigated iced airfoils over the years from different perspectives; the following paragraphs summarize their works.

Bragg, 1986. studied the aerodynamics of a National Advisory Committee for Aeronautics (NACA) 0012 airfoil with a simulated glaze ice accretion and he found that there is a decreasing in lift and increasing in the drag. **Bragg, 1994.**studied experimentally the aerodynamics of a NACA 0012 of 30-degree swept and unswept semi-span wing with simulated glaze ice accretion on their leading edge. He found in the region of 2D flow that all small roughness produced by the presence of the dense mid-span tap row caused higher than expected (C_D) results for the clean wing when the wake probe was placed directly behind the mid-span tap row. **National technical information service (NTIS), 2000** reported an integrated experimental and computational investigation to determine the effect of simulated ridge ice shapes on airfoil aerodynamics. **Mateescu, 2004.**presented an efficient solution of steady and unsteady flows by solving the Euler and Navier-Stokes equations using finite difference and finite volume formulations. **Mateescu and Abdo, 2005.** studied analytically the velocity and pressure distributions on airfoils of arbitrary shapes, considering the rigorous boundary conditions. A second-order accurate method using velocity singularities in the expression of the fluid velocity is first developed for airfoils in inviscid incompressible flows, by simultaneously solving the symmetric and anti-symmetric flow components defined by coupled complex boundary conditions. **Broeren, et.al, 2006.**carried out the flow field measurements on the upper surface of a GLC-305 airfoil configured with glaze and rime ice-shape simulations. The separation region for the glaze ice configuration was much larger than those for the rime ice case, resulting from the differences in the ice horn geometry. Changes in Reynolds number did not significantly affect the separation region characteristics. A larger Mach number resulted in a slightly larger separation region for the glaze ice case at α equal to 6^o. **Hasoun, 2007.** conducted to study the effect of simulated ice accreted on airfoil aerodynamics performance NACA 0012.

Bragg, et.al, 2008.conducted a major research program to improve the understanding of the aerodynamic scaling of ice accretions on airfoil NACA 23012. **Mirzaei,et.al,2008.**presented the icing phenomenon on surface of NLF-0414 airfoil experimentally using single element hot-wire and also using CFD calculations to solve Navier-Stokes equations, with 22.5 minute ice accretions at Reynolds number of 0.5×10^6. They concluded that Reynolds number variation did not affect seriously on the drag coefficient of iced airfoil. **Gord, et.al, 2009.** presented experimental and numerical analysis of incompressible flow around an airfoil NACA 0012.Numerical analysis combined vortex panel method techniques for solving potential flow around the airfoil and Von Karman boundary layer integral equation solver. Results show that this method has a good capability to predict velocity profile, pressure and drag coefficients over the surface. **Bortholin and Catalano, 2012.**analyzed two categories of icing accretions in NACA 0012 airfoil through the effects in the force as well as in pressure distribution via numerical simulations.

From above literature review, it can be seen that a rare of experimental investigations for iced symmetrical straight wings have been carried out for one ice shape (i.e. they didn't compared the effect of different shapes with each other on the same airfoil). Most of the reviewed researches were investigated numerically especially that of the glaze iced because it is natural complicated throughout the accretions on the airfoil. As a result concluded that aerodynamics performance of the airfoil affected by ice amount, shape and its location, also Angel Of Attack (AOA) and the geometry of the wing play important part as well. In addition most of previous studies indicated that ice accretion decreasing lift and increasing drag when the AOA increased.

The main objective of the present work is to investigate the aerodynamic characteristics of the iced and clean symmetrical wing (NACA0012airfoil) numerically and experimentally at zero and non-zero angle of attack. The CFD analysis of airfoil NACA 0012 is performed for a Reynolds number ($3.36*10^5$) at various angles of attack using a fully turbulent flow solution in ANSYS FLUENT software, where k-ε model and SIMPLE algorithm to solve the continuity and momentum equations of airflow over a 2D airfoil are adopted. Three shapes have been chosen as follow:

a. Horn iced shape (case A II).
b. Flat iced shape (case A III).
c. Quarter round forward iced shape (case A IV).

2. MATHEMATICAL MODEL ANDCOMPUTATIONAL METHODOLOGY

The two dimensional governing differential equations of external flow analysis in Cartesian coordinates with two equations for (k-ε) turbulence model **Verestage&Malalasekera, 1995.** can be written as:

- **Conservation of Mass**

$$\frac{\partial u}{\partial x} + \frac{\partial v}{\partial y} = 0 \quad \dots (1)$$

where u, υ are velocity components in x and y direction respectively.

- **Momentum Equations**

$$\frac{\partial}{\partial x}(\rho u u) + \frac{\partial}{\partial y}(\rho u \upsilon) = -\frac{\partial p}{\partial x} + \frac{\partial}{\partial x}(\mu_{eff}\frac{\partial u}{\partial x}) + \frac{\partial}{\partial y}(\mu_{eff}\frac{\partial u}{\partial y}) + S_u \quad (2)$$

v-momentum (y-direction)

$$\frac{\partial}{\partial x}(\rho \upsilon u) + \frac{\partial}{\partial y}(\rho \upsilon \upsilon) = -\frac{\partial p}{\partial y} + \frac{\partial}{\partial x}(\mu_{eff}\frac{\partial v}{\partial x}) + \frac{\partial}{\partial y}(\mu_{eff}\frac{\partial v}{\partial y}) + S_v \quad (3)$$

μ_{eff} is the effective viscosity coefficient which can be evaluated as:

$$\mu_{eff} = \mu_l + \mu_t \dots \quad (4)$$

where μ_l is the laminar viscosity, and μ_t is the turbulent eddy viscosity. S_u, is a source term of u in x-direction, while $S_v$is a source term of υ in y-direction.

The k-ε turbulence model is the two-equation model of kinetic energy (k) and its dissipation rate (**ε**) **Launder and Spalding1972**. This model relates the turbulent viscosity to the local values of ρ, k and ε by the expression.

$$\mu_t = \rho c_\mu k^2 / \varepsilon \quad (5)$$

wherec_μ is an empirical constant. The distribution of k and ε over the flow field is calculated from the following semi-empirical transport equations for k and ε , **Ideriah1975.**
(i) Turbulence Energy, k

$$\frac{\partial}{\partial x}(\rho u k) + \frac{\partial}{\partial y}(\rho \upsilon k) = \frac{\partial}{\partial x}(\frac{\mu_{eff}}{\sigma_k}\frac{\partial k}{\partial x}) + \frac{\partial}{\partial y}(\frac{\mu_{eff}}{\sigma_k}\frac{\partial k}{\partial y}) + G - \rho\varepsilon \quad (6)$$

(ii) Energy Dissipation Rate, ε

$$\frac{\partial}{\partial x}(\rho u \varepsilon) + \frac{\partial}{\partial y}(\rho \upsilon \varepsilon) = \frac{\partial}{\partial x}(\frac{\mu_{eff}}{\sigma_\varepsilon}\frac{\partial \varepsilon}{\partial x}) + \frac{\partial}{\partial y}(\frac{\mu_{eff}}{\sigma_\varepsilon}\frac{\partial \varepsilon}{\partial y}) + c_1\frac{\varepsilon}{k}G - c_2\rho\frac{\varepsilon^2}{k} \quad (7)$$

In the turbulence transport equations, Grepresents production of the kinetic energy from mean velocity gradients and σ_ε, $\sigma_k$are the effective Prandtl number.

$$G = \mu_t \{2[(\frac{\partial u}{\partial x})^2 + (\frac{\partial v}{\partial y})^2] + (\frac{\partial u}{\partial x} + \frac{\partial v}{\partial y})^2\} + S_G \quad (8)$$

$S_G$given by **Ideriah1975**.

$$S_G = -\frac{2}{3}\mu_t\left[\frac{\partial u}{\partial x} + \frac{\partial v}{\partial y}\right]^2 - \frac{2}{3}\rho k\left[\frac{\partial u}{\partial x} + \frac{\partial v}{\partial y}\right] \quad (9)$$

where S_G is source term of production of G.

The boundary conditions at the airfoil shown in **Fig. (1)** are:

- No slip boundary condition is applied on solid surface.
- Uniform and constant free stream velocity.
- The physical properties of air are constant.
- It is assumed that the ice formation is stretched from the wing root to the tip with no spanwise variations.

The Computational Fluid Dynamics (CFD) is adopted in this work by utilizing a finite volume method. Fluent software is used to solve the governing differential equations for air flow over a clean and iced airfoil. FLUENT does not contain an integrated meshing capability and must therefore be used with GAMBIT or other mesh generation software. Model construction, assembly and meshing require a trial and error approach that many times needs multiple iterations before a good geometry and mesh can be developed. **Fig. (2 a, b, c, and d**) represents the unstructured grid generated for airfoil with and without ice in Gambit, **Fluent Inc., 2009.**

3. EXPERIMENTAL WORK

The experimental investigation consisted of clean airfoil tests and ice shape castings (basically three shapes had been made) for aerodynamics testing. The aerodynamics characteristics investigation was made using a subsonic Low-Speed Wind Tunnel facility at the Mechanical engineering Dept.\ University of Baghdad. The wind tunnel used in the present work is a blowing type low speed, open circuit facility with solid walls and a maximum speed of 15.6 m\s. The general arrangement of this tunnel (experimental set up) is schematic in **Fig (3, a, b).** The test section is just downstream of the tunnel exit which its dimension is (450 mm high by 450 mm wide).The details of construction of the tunnel up to the test section are adopted from**, Hussain 1989.**

Aerodynamic considerations and facility size limitations determined the overall size of the wing model. Details of the symmetrical wing model and photograph for it are provided in **Fig (4, a, b).** The model is a symmetrical finite wing with a NACA 0012 two dimensional airfoil its coordinates are given in **Table (1),** airfoil section aligned in the streamwise direction. The airfoil section had manufactured from wood and had a maximum thickness to chord ratio of 0.12, the wing chord and span were 340 mm and 525 mm respectively. The model was instrumented with 16 pressure ports (suction and pressure side) distributed chordwise at one tap row spanwise locations corresponding to 50%, semispan which is aligned perpendicular to the stream direction and their coordinates are given in table (2)**,**

Bragg1994. The capillary tubes that are collected from the wing side face connected the pressure taps to the manometers.

Icing tests were conducted to document ice shapes formed on two-dimensional airfoils and to study the effects of the accreted ice on aerodynamic performance. The ice conditions were selected primarily from the Federal Aviation Administration's Federal Aviation Regulations **, Addy2000**. To verify the aerodynamic performance measurements, molds were made of selected ice shapes (three shapes were chosen) **, Addy2000.**and **FAA 2000**. Castings of the ice were made from wax and industrial clay because it is cheap and easy to form then horn ice shape and flat ice shape placed on the leading edge where the quarter round ice shape placed on the maximum thickness on the suction side of the symmetrical wing model in a dry low-speed wind tunnel, and precision aerodynamic performance measurements were taken. To illustrate how the castings look in general, **Fig (5, a, b)** shows the ice casting for the straight symmetrical airfoil.Pressure readings were obtained with a Pressure manometer System Inc. which by using the basic equation of pressure calculated to clean and iced airfoils at negative and positive angles of attack.

4. RESULTS AND DISCUSSION

The CFD analysis of airfoil NACA 0012 was performed for dimensionless chord section and Reynolds number ($3.63*10^5$) same as the experimental data at various angles of attack. To validate the adopted computational algorithm, the numerical results of this work are compared with previous work **, Rajakumar and Ravindran2012.** which analyze the flow over airfoil using the same boundary conditions. The maximum value of the percentage deviations obtained for lift and drag coefficient are (5.9%) at (17^o) AOA and (7.5%) at AOA (2^o). The coefficient of drag increases with the increase in angle of attack and it's not linear. Also the error percentage between the published results and present work was less than 10% of error.

Fig (6, a, b) shows pressure coefficient behavior over the upper and lower surfaces of the airfoil NACA 0012, it's obvious that there is a considerable decrease in pressure at the ice shape location on the upper surface because ice obstruct the streamline way and change the distribution of pressure over the airfoil. Also a reverse flow after ice location at the 35% of x/c on the upper surface of the airfoil NACA 0012 at angle of attack equal to (-12^o).

Fig (7, a) shows the variation of drag coefficient at different AOA for clean and iced symmetrical airfoil NACA 0012. The maximum drag reported for clean airfoil was (0.139) at angle of attack equal to (12^o). The most dangerous case is the horn iced (case A-II) which had the maximum percentage value of drag increased by (60%), while **Fig. (7, b)** presented C_l behavior for the clean and iced airfoil NACA 0012 at different angles of attack. It can be observed that lift coefficient of horn iced airfoil at AOA (12^o) is decreased by (38%). Fig. (7, c) shows numerical lift to drag coefficients ratio for clean and iced airfoil. The minimum value is equal to (3.6) at positive angle of attack. Numerical results of percentage reduction of lift coefficient and percentage increase of drag coefficient for iced cases at different angles of attack are given in **Table3.**

The velocity distribution over clean and iced airfoil at angle of attack equal to (4^o) is depicted in **Fig. 8.** No separation is indicated for case A-I (clean airfoil) and the maximum speed was (4 m/s) at the upper surface. For case (A-II) a reverse flow (bubble separation region) near ice location is indicated and the maximum speed at the upper surface was (4.3 m/s). This figure reveals two stagnation points for case A-IV one at the leading edge and the second at the quarter round iced shape.

Fig. 9. represents the distribution of computational pressure coefficient over clean and iced airfoil NACA 0012 at angle of attack (8^o). In case A-I the pressure on the lower surface of the airfoil was greater than that of the incoming flow. Also a back flow is reported at iced shapes location especially for horn iced case and quarter round forward iced shape case because of the shape of the ice and its location which considerably affect on the stream line of flow.

Four experimental cases are tested on symmetrical airfoil NACA 0012 with chord equal to **340 mm**, these cases are:

- Case A-I: Symmetrical clean airfoil.
- Case A-II: Horn iced symmetrical airfoil.
- Case A-III: Flat iced symmetrical airfoil.
- Case A-IV: Quarter round forward iced airfoil.

The experimental results of lift and drag coefficient at different angles of attack for the four cases for NACA0012 airfoil are given in **Table 4.** The maximum C_l is (0.92) for clean case at AOA (12^o). Horn iced airfoil produce the maximum drag at angle of attack equal to (12^o).**Fig.(10,a , b)** shows a comparison between the experimental results for the four cases (clean, flat iced, horn iced and quarter iced airfoil cases) at AOA (12^o). Case A-IV and case A-II reported the highest change in Cp distribution over the upper and lower surface of the airfoil compared to clean airfoil and this is due to the shape of the ice and the high AOA, where the maximum value of C_p is 0.51 at L.E., where x/c is equal to (0) for all cases.**Fig (11, a, b, c)** depicted the experimental conductance of the lift, drag coefficients and lift/drag ratio of NACA 0012 at different angles of attack for four cases. It shows that horn iced cause the maximum drag and minimum lift at positive angles of attack which is complies with previous literatures. The experimental percentage reduction and increase of lift coefficient and drag coefficient at different AOA for the studied cases above are given in **Table (5).**

Fig (12,a, b) represents the experimental power consumption due to drag force for clean and iced airfoil NACA 0012 at AOA (4^o, 8^o). The horn iced airfoil needs more power to avoid its effect than the other shapes of ice. It can be observed the maximum power is for horn iced airfoil, namely (44.4W) for NACA0012at AOA of (8^o). It can be observed at AOA (-4^o, -8^o) that the maximum power were for horn iced airfoil as (126W) for NACA0012at (-8^o) AOA. The power increases as the absolute value of negative AOA increase for each AOA.

A comparison between the numerical and experimental results of drag and lift coefficients are presented in **Fig. (13, a, b)** for clean airfoil (case A-I) at different angles of attack. It can be observed that experimental results had the same behavior of the numerical work with maximum deviation equal to (30%) and (10%) at AOA (12^o) for drag coefficient and lift coefficient respectively.

Fig (14, a, b) depicted a comparison between computational and experimental results of drag and lift coefficients for horn iced airfoil case NACA 0012 (case A-II) at different angles of attack. The drag coefficient C_d was almost identical at the negative angles but it mismatched at the positive angles it was less than the numerical results with maximum deviation equal to (35%) at angle of attack equal to (12^o), while the lift coefficient C_l had almost the same behavior of the numerical results with maximum deviation equal to (29%) at AOA (-12^o).

5. CONCLUSIONS

Experimental and computational investigations of the aerodynamic characteristics of an iced airfoil NACA 0012 at zero and non-zero angles of attack has been carried in this work. According to the previous discussion the following conclusions can be deduced:

- Experimental tests show that the presence of ice on airfoil increases drag by 60% and reduces lift by 45%. Horn iced airfoil consumes more power than the other shapes of ice.
- The numerical results show that the lift coefficient is decreased by 38% and the drag coefficient is increased by 60% for horn iced NACA 0012 airfoil.
- A steep pressure decrease is reported for iced airfoil with quarter round forward iced case at the location of ice (which was at the maximum thickness of the upper surface of the airfoil.
- Drag coefficient increases much higher for horn iced case compared to other cases of iced clean airfoil.
- For negative angle of attack (0^o, -4^o) the pressure coefficient (Cp) at iced airfoil airfoil lower surface was less than that of the upper surface.
- Prominent pressure spikes can be seen at the location of ice droplet on the airfoil surface.

REFERENCES

Addy H. E., 2000 *Ice Accretions and Icing Effects for Modern Airfoils*, NASA/TP-2000-210031, DOT/FAA/AR-99/89, April.

Bortholin T., Catalano F. M., 2012 *Computational investigation of icing contamination on airfoil*, 28th International Congress of the Aeronautical Sciences (ICAS).

Bragg M., 1986 *An experimental study of the aerodynamics of a NASA 0012 airfoil with simulated glaze ice accretion*, The Ohio State University Research foundation Columbus, Ohio prepared for NASA Lewis Research Centre under Grant No. NAG 3-28 CR 179897, November.

Bragg M., 1994 , *An experimental study of the aerodynamics of a swept and unswept semispan wing with a simulated glaze ice accretion*, prepared for Lewis Research Centre under Grant NAG 3-1134 NACA CR195330, University of Illinois-Urbana, May.

Bragg M., Broeren A.P., Addy H. E., Potapczuk M. G., 2008 ,*Airfoil Ice-Accretion Aerodynamics Simulation*, NASA/TM—2008-214830, AIAA–2007–0085.

Broeren A. P., Bragg M., Addy, 2006, *Flow field Measurements About an Airfoil with Leading-Edge Ice Shapes*, journal of aircraft Vol. 43, No. 4, July–August.

Federal Aviation Administration (FAA)., 2000, office of Aviation Research Washington, D.C. 20591, U.S. Department of Transportation, *Effects of Large-Droplet Ice Accretion on Airfoil and Wing Aerodynamics and Control*, National Technical Information Service (NTIS), Springfield, Virginia 22161, DOT/FAA/AR-00/14, March.

Fluent Inc., 2009 Fluent User's Guide, Version 6.3.26. *Available free online on www.sharcnet.ca.*

Gord M. F., 2009 Alizadeh H. H., *Combined Experimental and Numerical Analysis of Incompressible Flow around an Airfoil*, Shahrood University of Technology, Shahrood, Iran, computational dynamics, part 41, part , pp. 793-798.

Hasoun, H. Q., 2007 ,*Effect of ice formation on airfoils performance*, PH.D. thesis, university of Baghdad, College of Engineering, Dept. of Mech. Engr.

Hussain, I.Y., 1989 *Computational and experimental investigation of three dimensional turbulent boundary layer*, M.Sc. thesis, university of Baghdad, college of Engineering, Dept. of Mech. Engr,.

Ideriah, F. J. K., 1975, *Review of equation solved in TEACH*, private communication.

Launder, B.E. and Spalding, D.B., 1972, *Mathematical models of turbulence*, Academic press, London.

Mateescu D., 2004 *Efficient solution of the Euler and Navier-stokes equations for external flow*, the 6th International Conference on Hydraulic Machinery and Hydrodynamics (H M H), Timisoara, Romania, October 21 - 22.

Mateescu D., 2005Abdo M., *Efficient second-order analytical solutions for airfoils in subsonic flows*, Aerospace Science and Technology 9 pp. 101–115. Also vailable online on www.sciencedirect.com.

Mirzaei M., Ardekani M. A., Doosttalab M., 2008 , *Numerical and experimental study of aerodynamic characteristics of an iced airfoil*, 5th WSEAS Int. Conf. on fluid mechanics (fluids'08) Acapulco, Mexico, January 25-27.

National technical information service (NTIS)., 2000 *Effects of Large-Droplet Ice Accretion on Airfoil and Wing Aerodynamics and Control*, spring field, Virginia 22161, March.

Rajakumar S., Ravindran D., 2012 ,*Iterative approach for optimising coefficient of power, coefficient of lift and drag of wind turbine rotor*, Anna university of technology, India, available online at Science Direct, Renewable energy 38, pp. 83-93.

Verestage, H. K., and Malalasekera, W., 1995 *An Introduction to Computational Fluid Dynamic-The Finite volume Method*, Longman Group Ltd.

Nomenclature

Latin symbols		**Greek symbols**	
AR	Aspect Ratio	α	Angle of attack Deg.
b	Span length of wingm	∞	Mainstream conditions
C_1, C_2, $C\mu$	constants for (k-ε) model	λ	Taper ratio
C_d	Drag Coefficient	ε	Rate of dissipation of kinetic energy m^2/s^3
C_l	Lift coefficient	μ	Dynamic viscosity N.s/m^2
Cp	Pressure coefficient [(P-Pa)/0.5ρV_∞^2]	μ_l	Laminar viscosity N.s/m^2
G	Production of the kinetic energy from mean velocity gradients	μ_t	Turbulent viscosity N.s/m^2
k	Kinetic energy of turbulence m^2/s^2	μ_{eff}	Effective kinematics viscosity N.s/m^2
		ρ	Density Kg/m3
p	PressurePa	σ_k, σ_ε	constants for (k-ε) model
q_∞	Reference pressure [0.5ρV_∞^2] N/m^2	**Abbreviations**	
Re	Reynolds number	AOA	Angle Of Attack
S	Surface wing area m^2	CFD	Computational Fluid Dynamics
SG	Source term of production of the kinetic energy from mean velocity gradients	CV	Control Volume
Su	Source term of u in x-direction,	2D	Two-Dimensional
		FAA	Federal Aviation Administration
Sv	Source term of υ in y-direction	FVM	Finite Volume Method
u ,v	Velocity component in x, y respectively m/s	IRT	Icing Research Tunnel
		L.E	Leading Edge
V∞	Free stream velocity m/s	NTIS	National Technical Information Service
x, y	Cartesian coordinates	SIMPLE	Semi-Implicit Method for Pressure Linked Equation
		T.E	Trailing Edge

Table 1. Symmetrical straight airfoil coordinates.

No.	x/c	y/c	No.	x/c	y/c	No.	x/c	y/c
1	1	0.00126	25	0.224552	0.058578	49	0.303487	-0.06001
2	0.997987	0.001542	26	0.188255	0.056645	50	0.345492	-0.05958
3	0.991965	0.002382	27	0.154469	0.053896	51	0.38874	-0.05843
4	0.981981	0.00376	28	0.123464	0.050351	52	0.432883	-0.05665
5	0.968117	0.005647	29	0.095492	0.046049	53	0.477568	-0.0543
6	0.950484	0.008002	30	0.070776	0.041043	54	0.522432	-0.05147
7	0.929224	0.010776	31	0.049516	0.0354	55	0.567117	-0.04824
8	0.904508	0.013914	32	0.031883	0.029189	57	0.61126	-0.0447
9	0.876536	0.017359	33	0.018019	0.022483	58	0.654508	-0.04092
10	0.845531	0.021049	34	0.008035	0.015347	59	0.696513	-0.03698
11	0.811745	0.024921	35	0.002013	0.007839	60	0.736934	-0.03295
12	0.775448	0.02891	36	0	0	61	0.775448	-0.02891
13	0.736934	0.032952	37	0.002013	-0.00784	62	0.811745	-0.02492
14	0.696513	0.036978	38	0.008035	-0.01535	63	0.845531	-0.02105
15	0.654508	0.040917	39	0.018019	-0.02248	64	0.876536	-0.01736
16	0.61126	0.044698	40	0.031883	-0.02919	65	0.904508	-0.01391
17	0.567117	0.048243	41	0.049516	-0.0354	67	0.929224	-0.01078
18	0.522432	0.051471	42	0.070776	-0.04104	68	0.950484	-0.008
19	0.477568	0.0543	43	0.095492	-0.04605	69	0.968117	-0.00565
20	0.432883	0.056646	44	0.123464	-0.05035	70	0.981981	-0.00376
21	0.38874	0.05843	45	0.154469	-0.0539	71	0.991965	-0.00238
22	0.345492	0.059575	46	0.188255	-0.05665	72	0.997987	-0.00154
23	0.303487	0.060014	47	0.224552	-0.05858	73	1	-0.00126
24	0.263066	0.059695	48	0.263066	-0.0597			

Table 2. Pressure taps coordinates.

No.	X mm	Y mm
1	0	0
2	10.37	9.7268
3	19	12.6537
4	36.7	16.3458
5	71.7	19.6895
6	105.19	20.375
7	140	19.5463
8	173.16	17.766
9	206.6	15.2648

Table 3. Numerical precentage reduction and incease of lift and drag coefficients for NACA 0012.

	Case A	AOA					
		4	8	12	-4	-8	-12
% reduction of lift coefficient	II	5	20	20.565	1.47	6.35	6.56
	III	3	3.5	6.6	4.52	7.338	12.85
	IV	6.6	12	13.5	2.68	4.961	3.7
% increase of drag coefficient	II	34.7	38.67	68	40.8	63	75.48
	III	9	15.4	26.1	17.78	22.98	28.9
	IV	6	7.37	38.2	11.66	28.11	39.6

Table 4. Experimental lift and drag coefficients for NACA 0012 airfoil.

	Case A	AOA						
		0	4	8	12	-4	-8	-12
Lift coefficient	I	0.017	0.29	0.614	0.92	-0.459	-0.74	-0.9
	II	0.001	0.259	0.537	0.769	-0.194	-0.597	-0.85
	III	0.011	0.27	0.61	0.89	-0.39	-0.71	-0.87
	IV	0.011	0.26	0.59	0.875	-0.35	-0.72	-0.885
Drag coefficient	I	0	0.019	0.045	0.085	0.051	0.083	0.125
	II	0	0.03	0.056	0.087	0.075	0.159	0.263
	III	0	0.022	0.049	0.074	0.069	0.135	0.185
	IV	0	0.02	0.046	0.085	0.04	0.135	0.235

Table 5. Experimental precentage reduction and incease of lift and drag coefficients.

	Case A	AOA					
		4	8	12	-4	-8	-12
% Reduction of lift coefficient	II	11.6	12.5	16.2	57.79	19.31	5.55
	III	2.54	2.39	3.1	15.18	4.05	3.3
	IV	3.57	4	4.7	23.87	2.7	1.66
% Increase of drag coefficient	II	16.35	15.6	23.27	45.13	48.1	52.18
	III	3.97	4.7	4.84	33.87	58.5	47.17
	IV	5.75	2.75	20.4	22.39	58.5	86.95

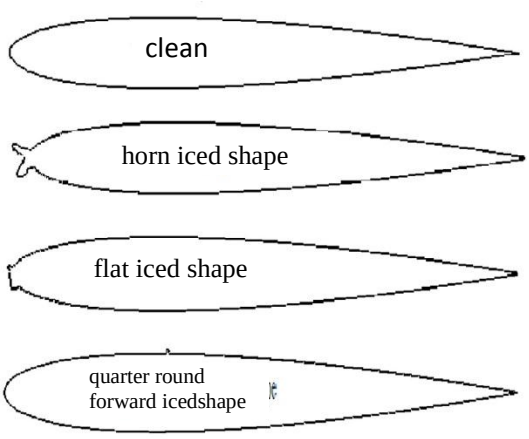

Figure 1. Airfoil profile with and without ice.

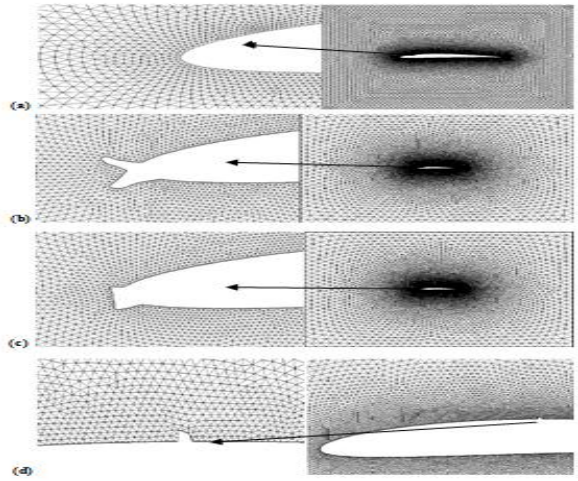

Figure 2. Mesh for airflows over airfoil NACA 4410. a) clean airfoil, b) horn iced airfoil, c) flat iced airfoil, d) quarter round forward iced airfoil.

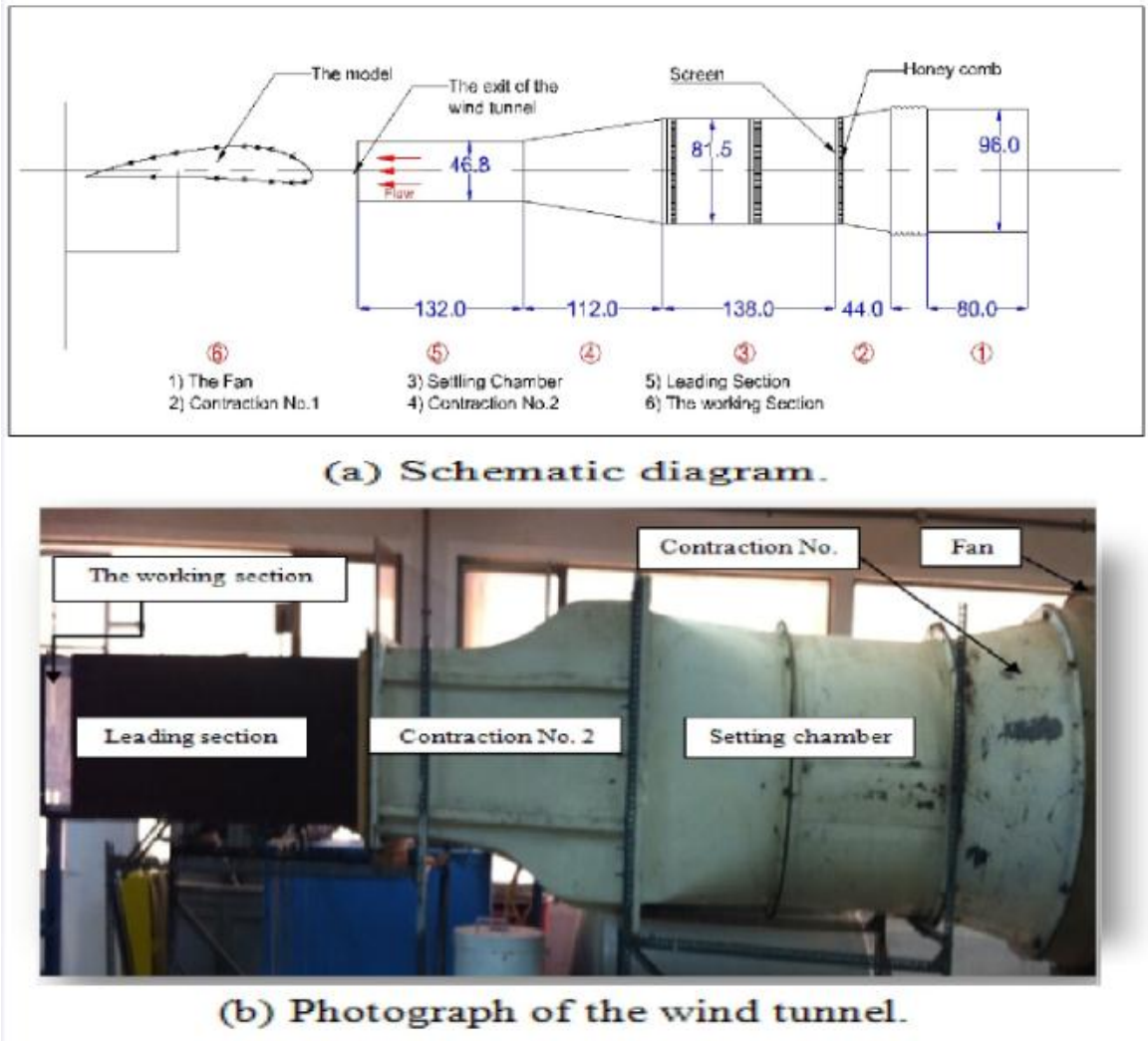

Figure 3. Subsonic wind tunnel at Mechanical Engr. Dept.

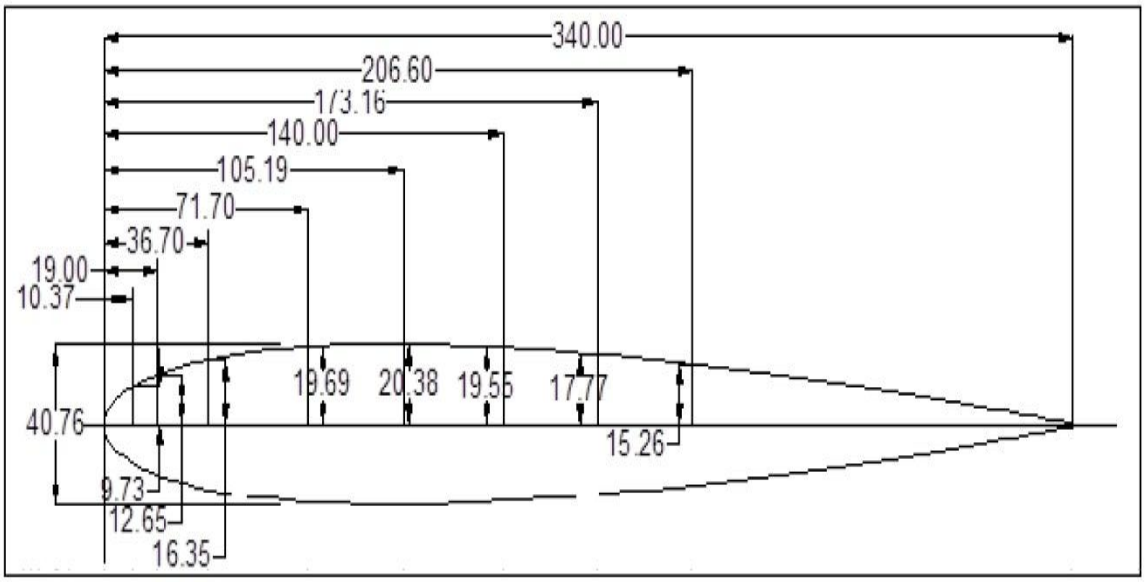

(a)

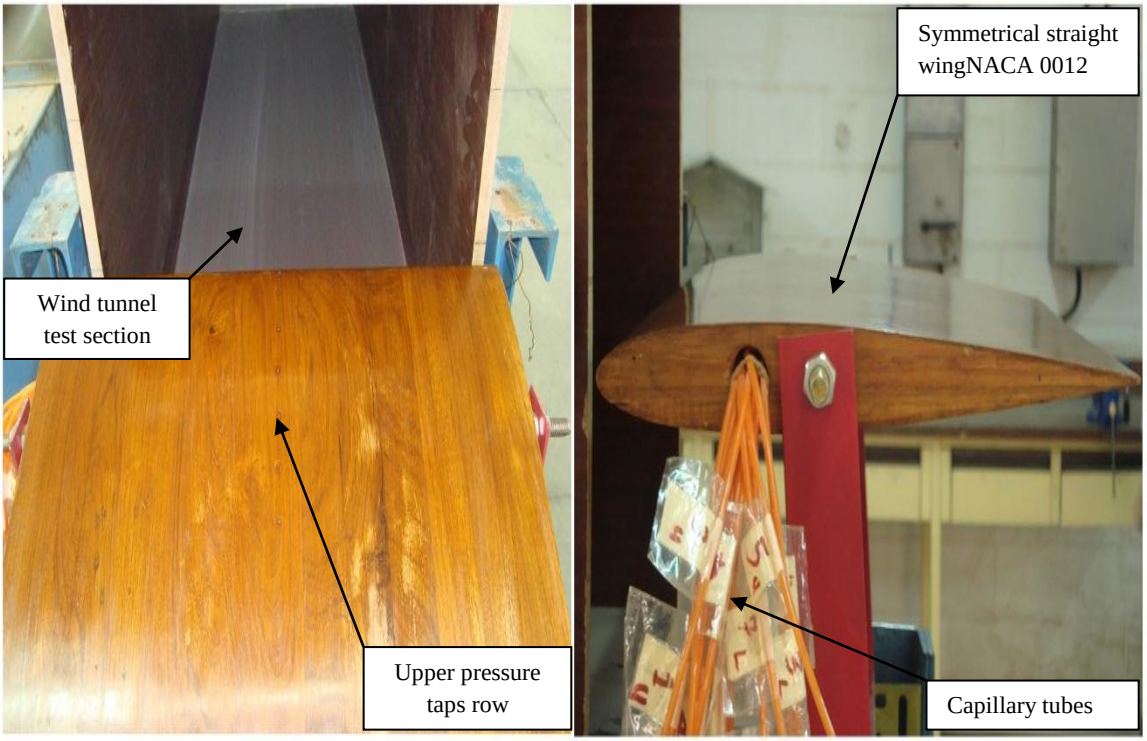

(b)

Figure 4. The symmetrical wing model, (a) Designed section and pressure taps arrangement(all dimensions in mm), (b) Photographs of the straight wing side and top view.

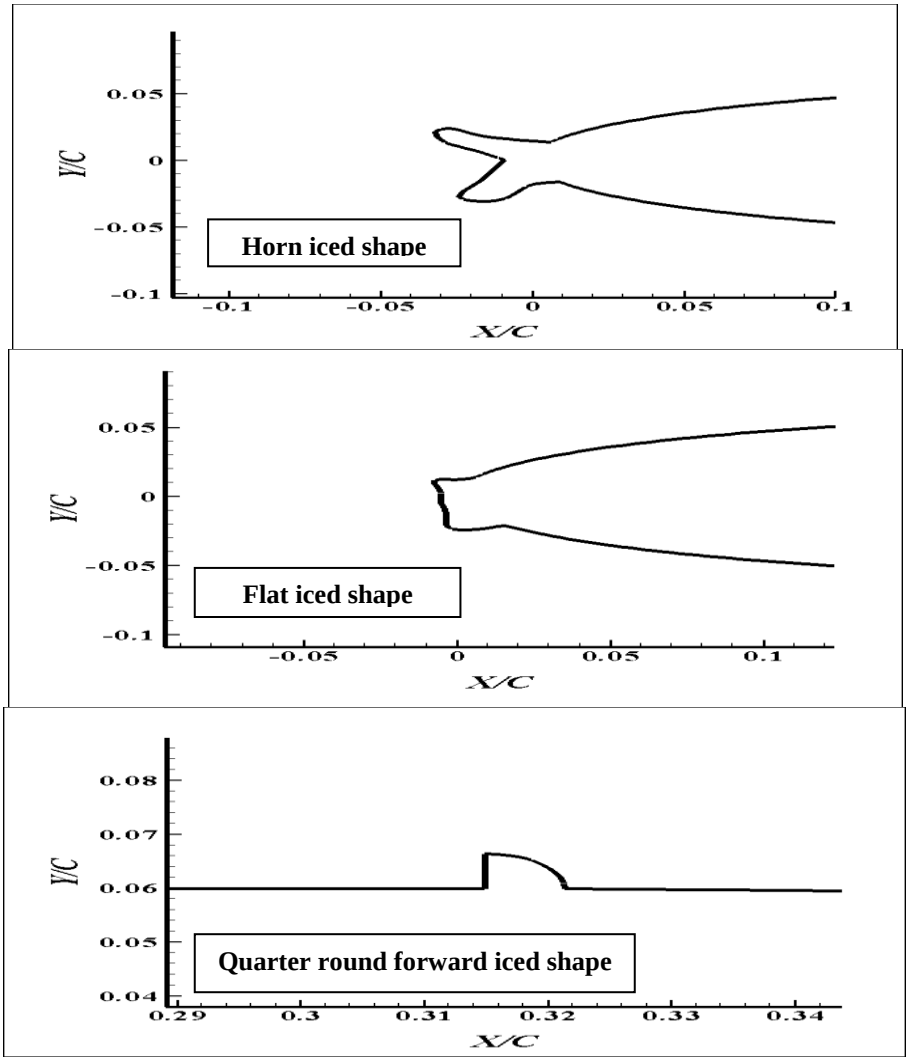

(a)

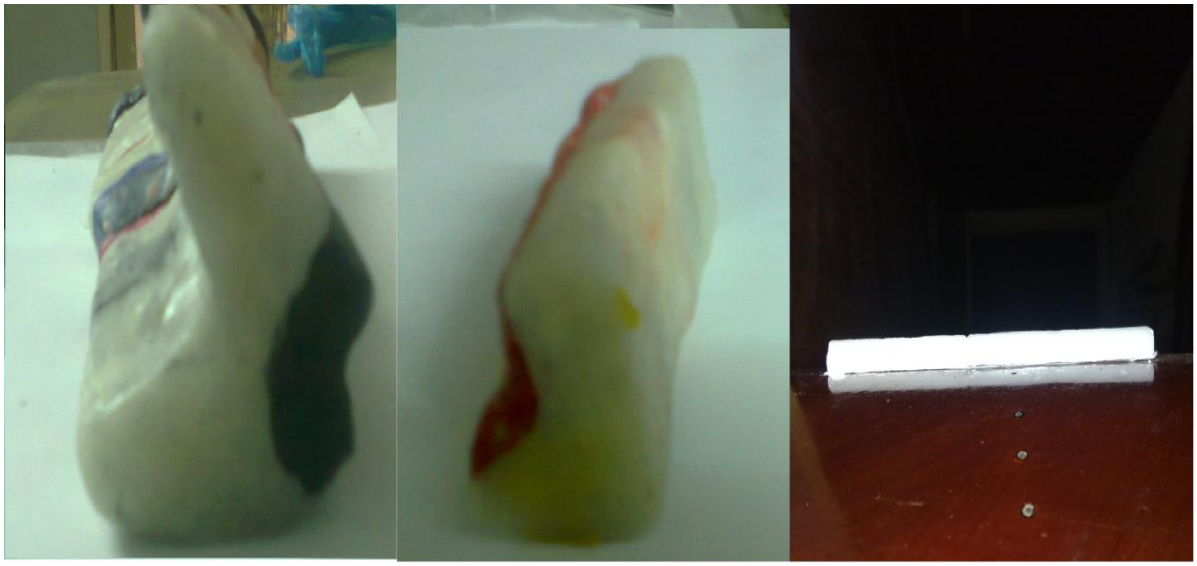

(b) **Figure 5.** The ice casting for the straight symmetrical airfoil, (a) Typical iced shapes, (b) photographs for three iced shapes.

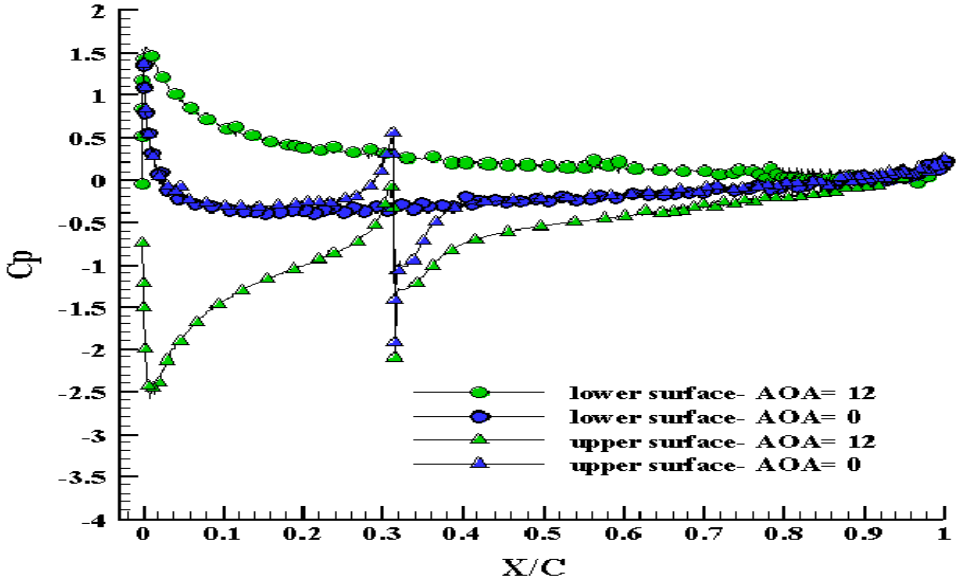

(a)

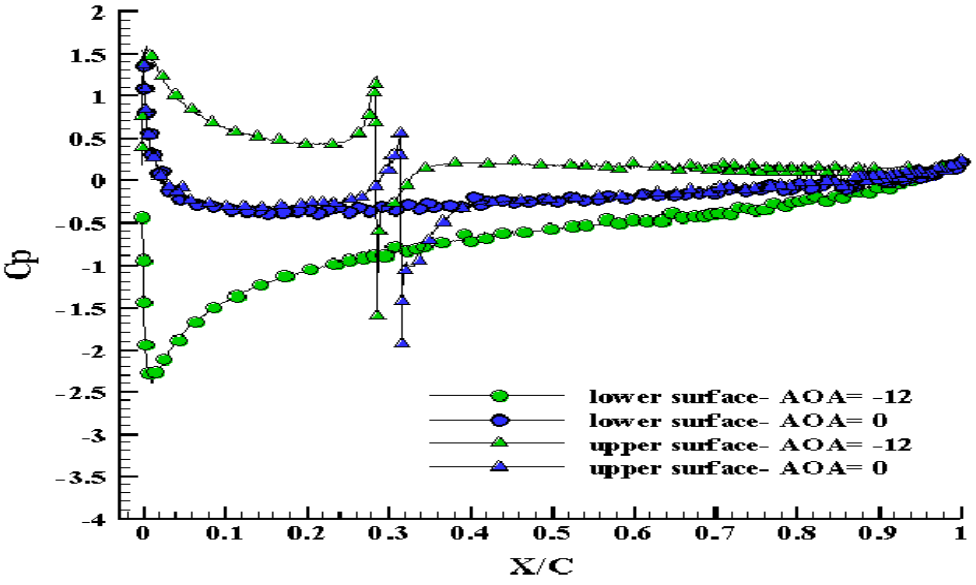

(b)

Figure 6. Pressure coefficient distribution of quarter round forward iced airfoil NACA 0012 at, (a) AOA (0°, 12°), (b) AOA (0°, -12°).

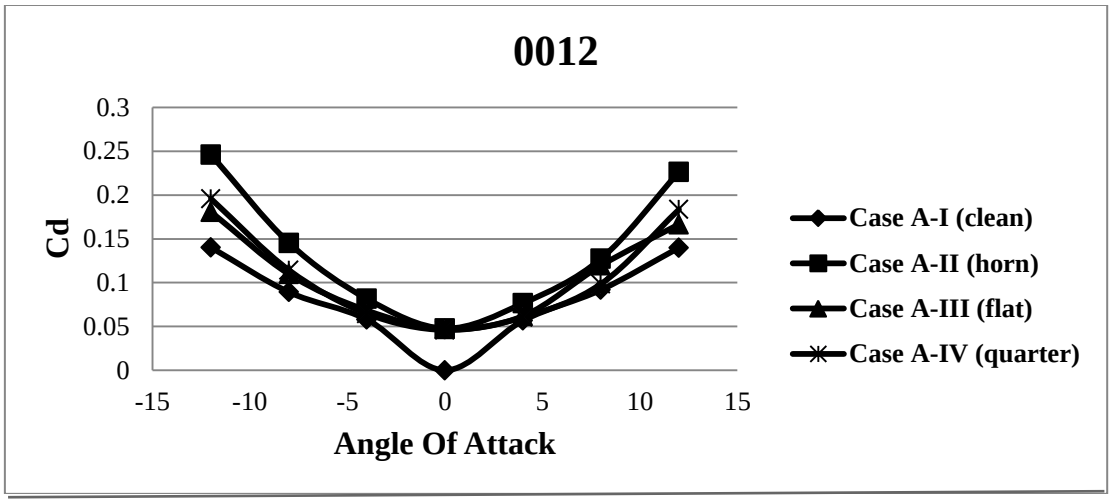

(a)

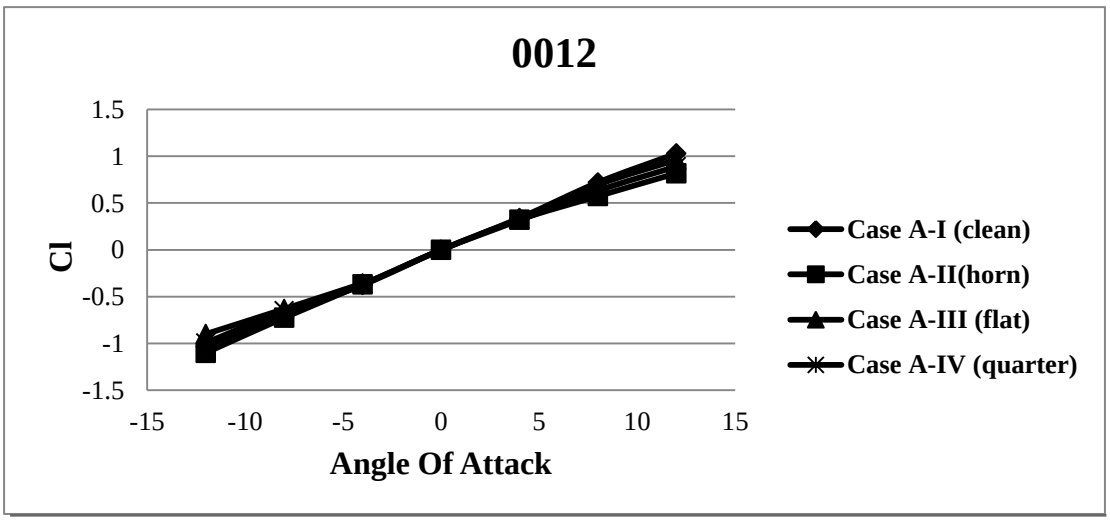

(b)

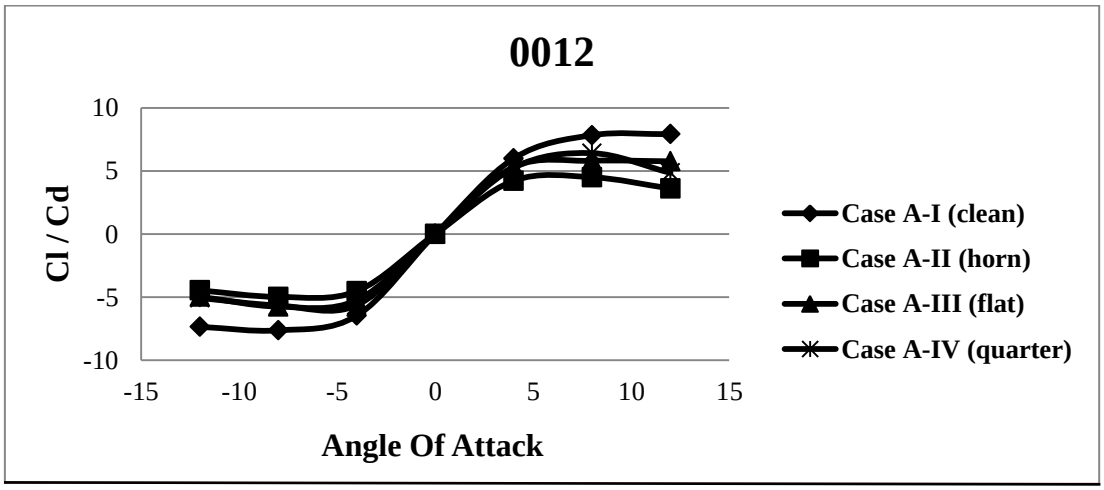

(c)

Figure 7. Numerical results for NACA 0012 at different AOA, (a) Cl, (b) Cd, (c) Cl/Cd.

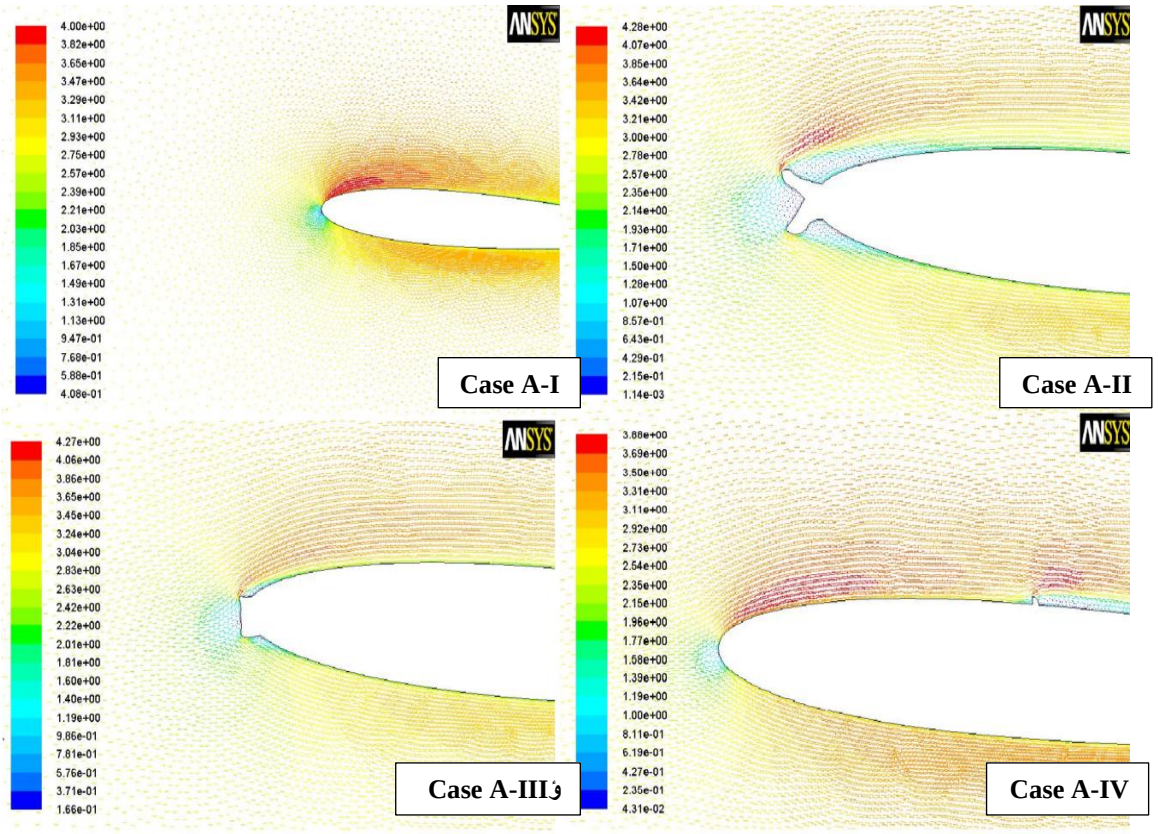

Figure 8. Velocity distribution for clean and iced airfoil at angle of attack (4°).

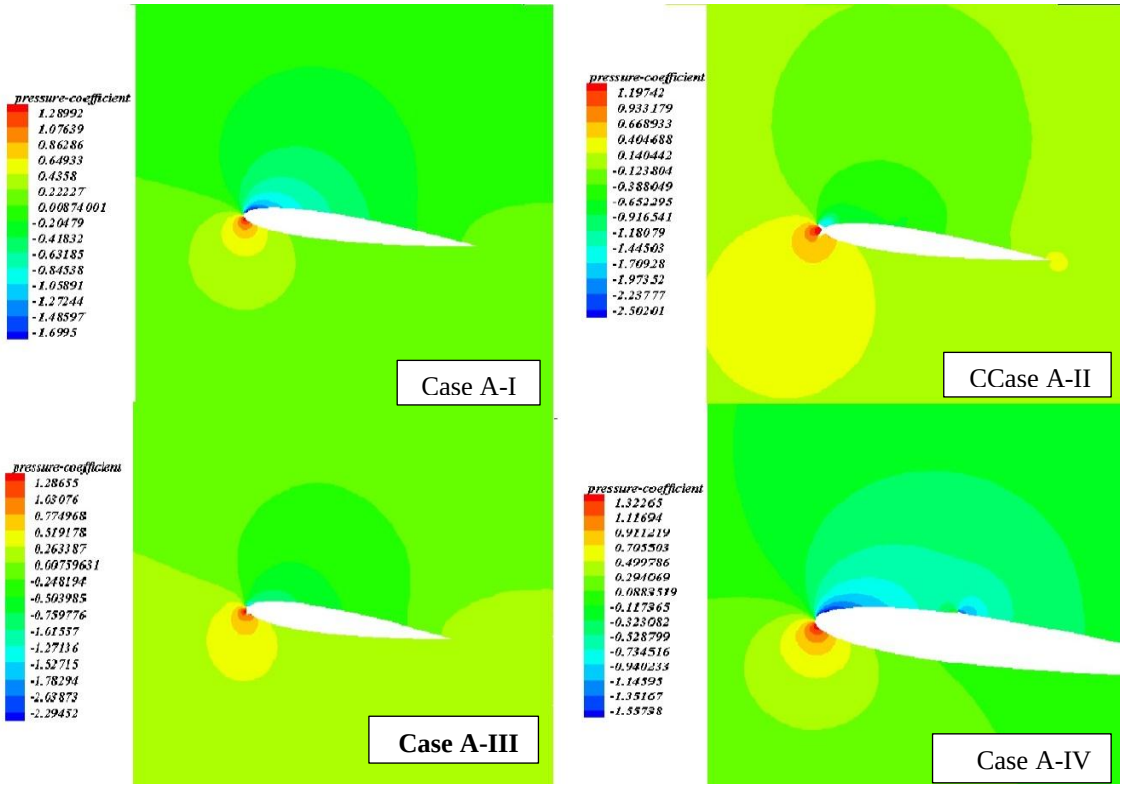

Figure 9. Pressure coefficient distribution over clean and iced airfoil NACA 0012 at angle of attack (8^{o}).

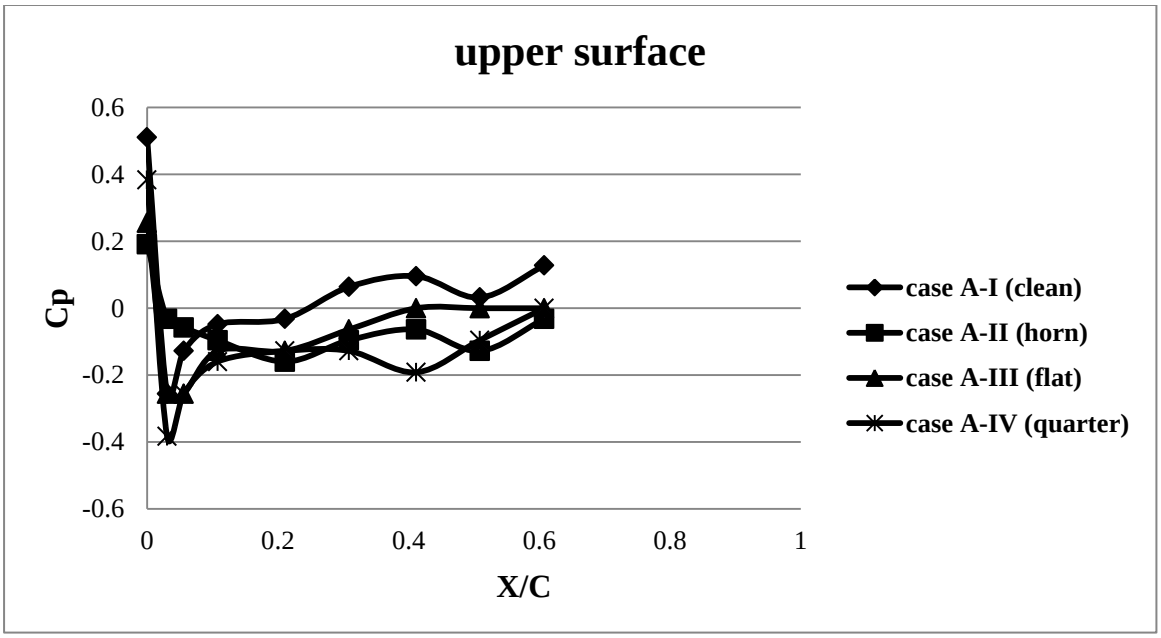

(a)

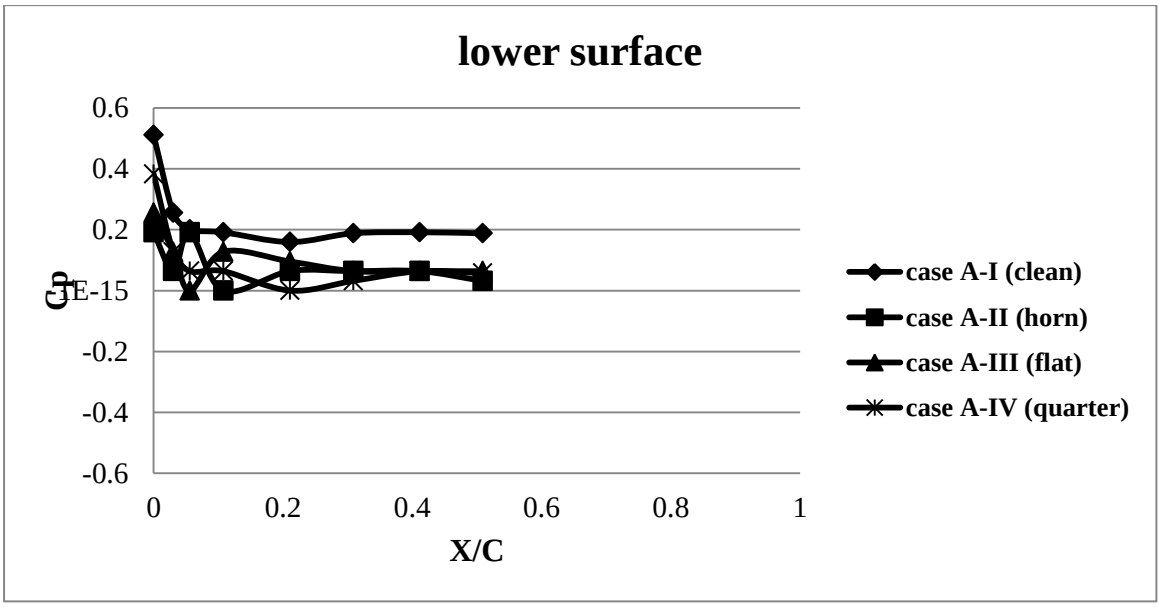

(b)

Figure 10. Pressure distribution of symmetrical airfoil NACA 0012 with chord equal to (340 mm) at AOA (12^{o}) for different experimental cases, (a) upper surface, (b) lower surface.

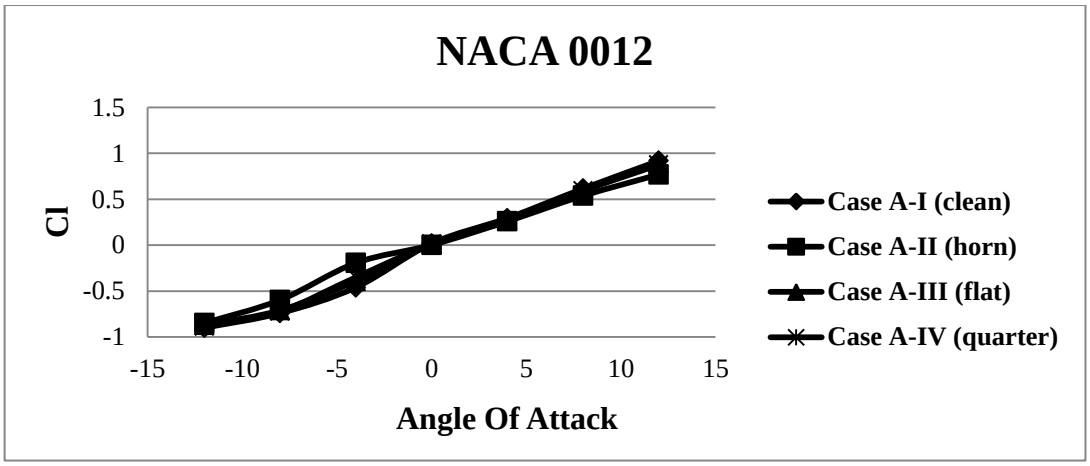

(a)

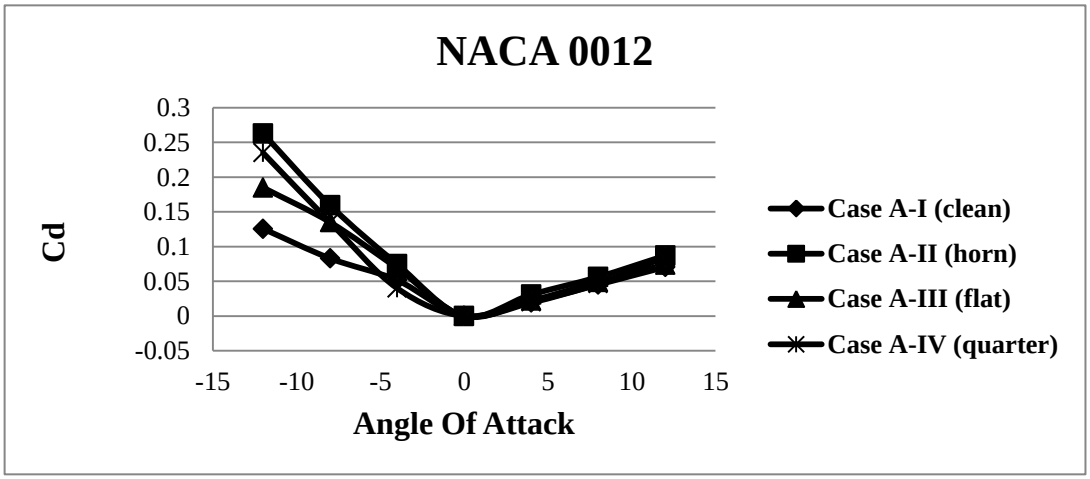

(b)

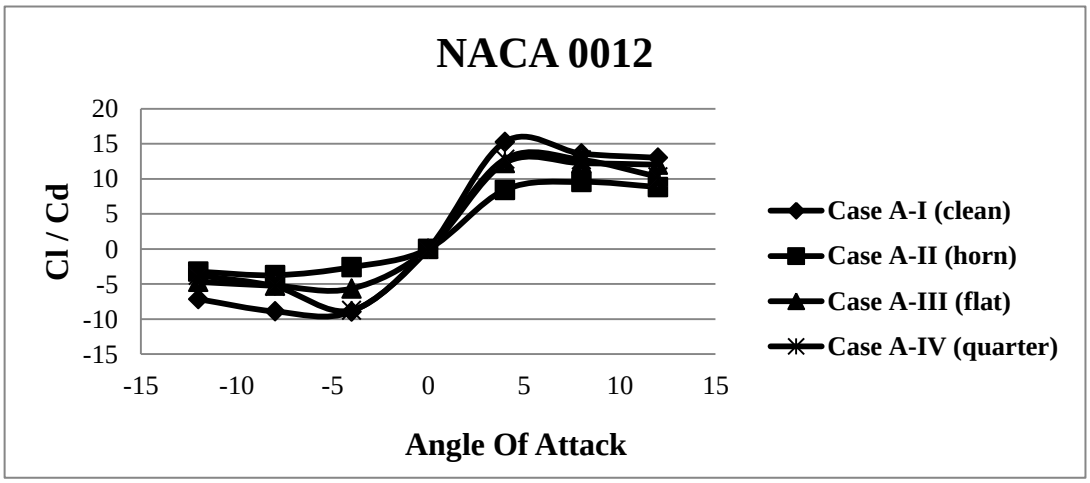

(c)

Figure 11. Experimental results for NACA 0012 at different AOA, (a) Cl, (b) Cd, (c) Cl/Cd.

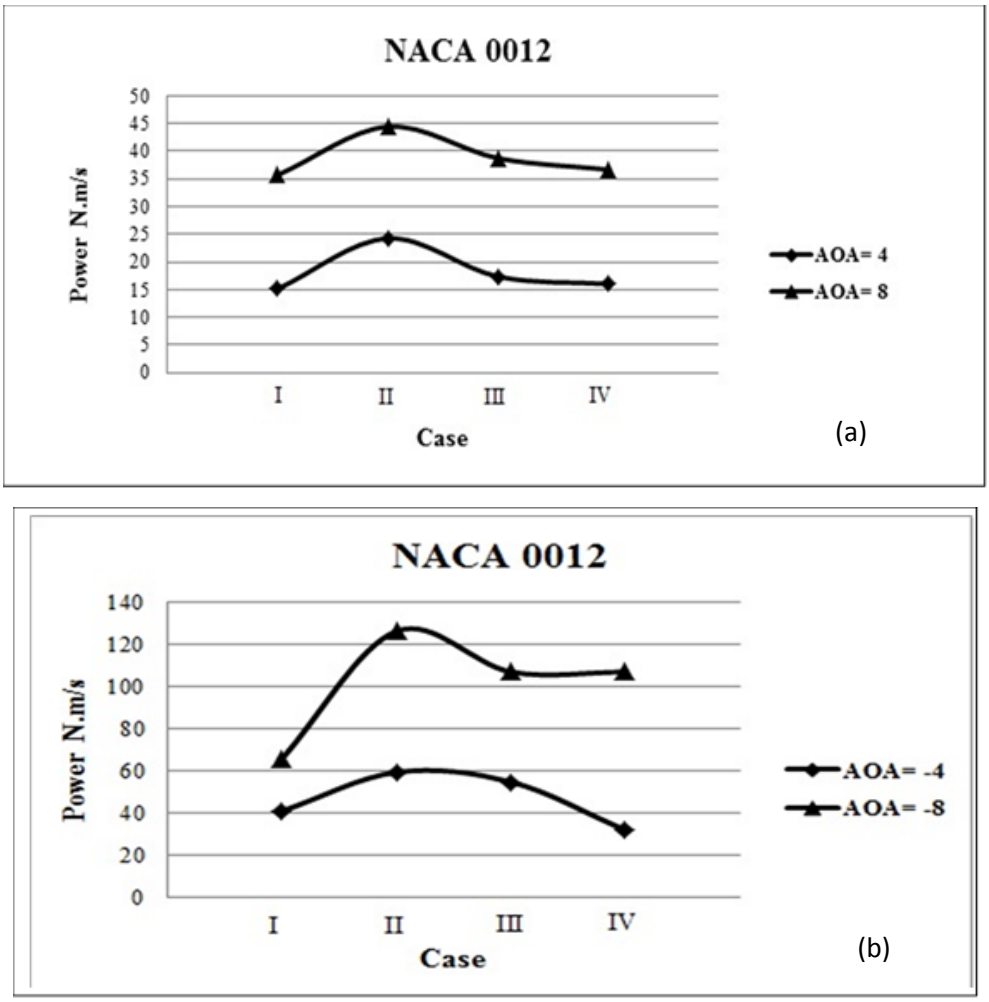

Figure 12. Power consumption due to drag force for clean and iced airfoil NACA 0012
At (a) AOA (4˚, 8˚), (b) AOA (-4˚, 8˚).

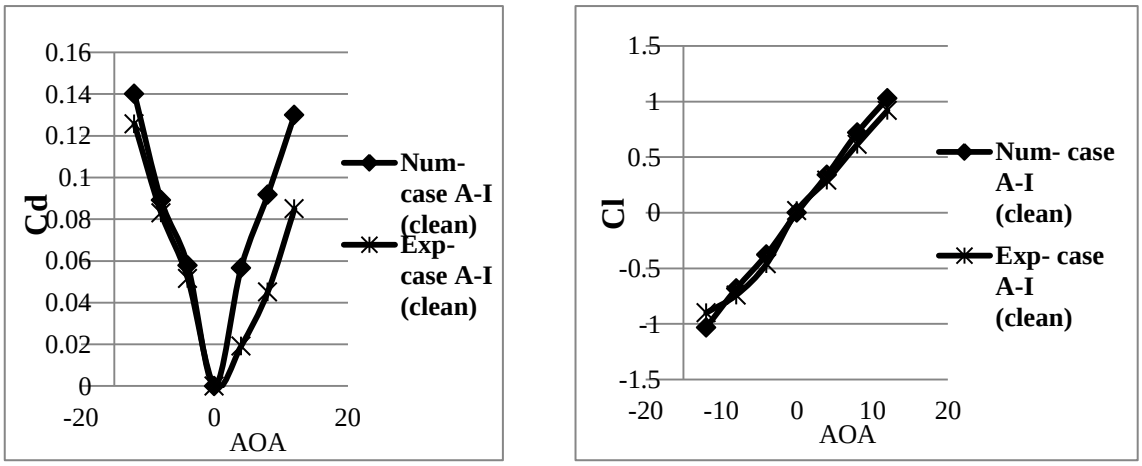

Figure 13. Comparison between the numerical and experimental results for clean case NACA0012 at different angles of attack, (a) Drag coefficient, (b) Lift coefficient.

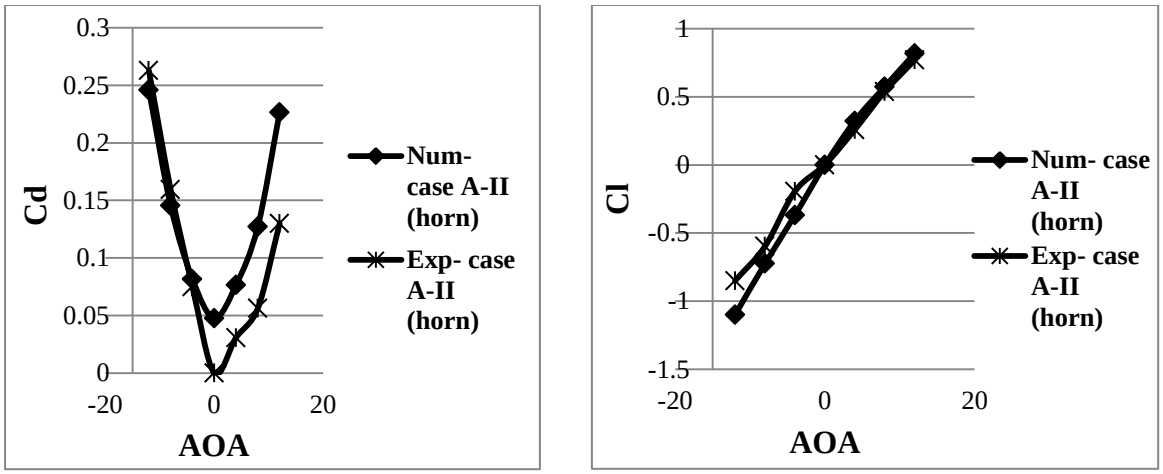

(a) (b)

Figure 14. A comparison between the numerical and experimental results for horn iced airfoil case NACA0012 at different angles of attack, (a) Drag coefficient, (b) Lift coefficient.